Dynamics of magma chamber replenishment under buoyancy and pressure forces

Antonella Longo[1], Deepak Garg[2], Paolo Papale[1], and Chiara Paola Montagna[1]

[1]Istituto Nazionale di Geofisica e Vulcanologia
[2]Istituto Nzionale di Geofisica e Vulcanologia

November 24, 2022

Abstract

Active magma chambers are periodically replenished upon a combination of buoyancy and pressure forces driving upward motion of initially deep magma. Such periodic replenishments concur to determine the chemical evolution of shallow magmas, they are often associated to volcanic unrests, and they are nearly ubiquitously found to shortly precede a volcanic eruption. Here we numerically simulate the dynamics of shallow magma chamber replenishment by systematically investigating the roles of buoyancy and pressure forces, from pure buoyancy to pure pressure conditions and across combinations of them. Our numerical results refer to volcanic systems that are not frequently erupting, for which magma at shallow level is isolated from the surface (â\euroœclosed conduitâ\euro? volcanoes). The results depict a variety of dynamic evolutions, with the pure buoyant end-member associated with effective convection and mixing and generation of no or negative overpressure in the shallow chamber, and the pure pressure end-member translating into effective shallow pressure increase without any dynamics of magma convection associated. Mixed conditions with variable extents of buoyancy and pressure forces illustrate dynamics initially dominated by overpressure, then, over the longer term, by buoyancy forces. Results globally suggest that many shallow magmatic systems may evolve during their lifetime under the control of buoyancy forces, likely triggered by shallow magma degassing. That naturally leads to long-term stable dynamic conditions characterized by periodic replenishments of partially degassed, heavier magma by volatile-rich fresh deep magma, similar to those reconstructed from petrology of many shallow-emplaced magmatic bodies.

Dynamics of magma chamber replenishment under buoyancy and pressure forces

A. Longo[1], D. Garg[1], P. Papale[1], and C.P. Montagna[1]

[1]Istituto Nazionale di Geofisica e Vulcanologia, Sezione di Pisa, Via Cesare Battisti 53, 56125 Pisa, Italy

Key Points:

- A numerical model for time-space dynamics in shallow magma chambers replenished by deep magma is presented
- Evolution under pressure and buoyancy forces is initially dominated by overpressure, and over the long-term by buoyant convection and mixing
- Lifetime evolution of volcanic systems is likely towards stable conditions with no pressure build-up leading to an eruption

Corresponding author: Antonella Longo, `antonella.longo@ingv.it`

Abstract

Active magma chambers are periodically replenished upon a combination of buoyancy and pressure forces driving upward motion of initially deep magma. Such periodic replenishments concur to determine the chemical evolution of shallow magmas, they are often associated to volcanic unrests, and they are nearly ubiquitously found to shortly precede a volcanic eruption. Here we numerically simulate the dynamics of shallow magma chamber replenishment by systematically investigating the roles of buoyancy and pressure forces, from pure buoyancy to pure pressure conditions and across combinations of them. Our numerical results refer to volcanic systems that are not frequently erupting, for which magma at shallow level is isolated from the surface ("closed conduit" volcanoes). The results depict a variety of dynamic evolutions, with the pure buoyant end-member associated with effective convection and mixing and generation of no or negative overpressure in the shallow chamber, and the pure pressure end-member translating into effective shallow pressure increase without any dynamics of magma convection associated. Mixed conditions with variable extents of buoyancy and pressure forces illustrate dynamics initially dominated by overpressure, then, over the longer term, by buoyancy forces. Results globally suggest that many shallow magmatic systems may evolve during their lifetime under the control of buoyancy forces, likely triggered by shallow magma degassing. That naturally leads to long-term stable dynamic conditions characterized by periodic replenishments of partially degassed, heavier magma by volatile-rich fresh deep magma, similar to those reconstructed from petrology of many shallow-emplaced magmatic bodies.

1 Introduction

Magmatic systems below active volcanoes can be extremely complex in terms of their shape, physical properties, and evolution (Tibaldi, 2015; Burchardt et al., 2016; Cashman et al., 2017; R. S. J. Sparks & Cashman, 2017; R. Sparks et al., 2019; R. S. J. Sparks et al., 2022). Magmatic systems can extend vertically over several km, with the shallower portions located only a few km, sometimes less than 1 km, below the surface, connected through dyke systems to other reservoirs at different depths, and often to a larger one at depths approaching or exceeding 10 km (references above). The shallow portion of such composite magmatic systems is typically more chemically evolved and partially degassed with respect to the deeper magma, as a result of inter-dependent processes such as cooling, crystallization and degassing that are more efficient at shallow depth. Long lifetime to such shallow magmatic bodies, much in excess of estimated conductive cooling lifetimes, is provided by repeated magma injection events (Marsh, 2015) which add mass, heat, and volatiles, thus contrasting shallow-level cooling and degassing. Events of new injection at shallow level by deeper, chemically and physically distinct magma are often recognized to have shortly preceded the occurrence of a volcanic eruption (Colucci & Papale, 2021, and references therein). The dynamics associated with magma injection at shallow level are the subject of this work.

The motion of a fluid, from single-phase single component (such as pure water) to multi-phase multi-component such as natural magma, relates to either natural or forced convection, or to a combination of them. Natural convection arises because fluids are immersed in the gravitational field, causing lighter portions to move up while denser portions sink down. The existence of density differences is therefore the cause of natural convection. In the case of real magmas, the melt phase of less chemically evolved (deeper) magmas tends to be denser than their evolved, shallow counterpart, as a reflection of larger content of heavy metals and lower content of light silicon more than compensating for higher temperature (Lange & Carmichael, 1990). Larger contents of heavy crystals such as olivine and pyroxene add to the density excess by more mafic magmas. However, shallow magmas get degassed as a reflection of the largely dominant role of pressure on volatile saturation. In particular, the largely insoluble carbon dioxide component is quickly lost at shallow depth. Because the presence of carbon dioxide causes more water exsolution and the generation of a larger volume of gas at equal other conditions (Papale et al., 2022), and because of the order of magnitude difference, increasing with decreasing pressure thus depth, between the density of the melt+crystals and gas phases, it follows that magmas coming from depth are easily lighter than the more evolved, partially degassed magmas they encounter at shallower depth, giving rise to natural convection.

In contrast with natural convection, forced convection relates to fluid motion governed by forces different from buoyancy. An example of forced convection is fluid motion inside a blender, or the motion of air in a room when a hair dryer is turned on (more precisely, the latter is a combination of natural and forced convection as the density of the air exiting the hair dryer is normally lower than ambient density). In magmatic environments, forced convection can arise as a consequence of chemical processes causing phase changes within confined systems leading to pressure increase, stress accumulation by local or regional tectonics, or by mantle or subduction dynamics. In all cases, forced convection requires the build-up of exceeding pressure somewhere in the system.

Magma motion is invariably associated with either a density difference, or some other force resulting in a pressure difference. Accordingly, deep magma can intrude a shallow reservoir either because it is lighter than the magma hosted in the reservoir (buoyancy force), or because it is pushed from below (pressure force), or because of a combination of both. Here we examine the entire spectrum from pure buoyancy (the end-member case analyzed in Papale et al. (2017)) to pure pressure triggering magma injection, through variable combinations of buoyancy and pressure. We describe markedly different system evolutions under the analyzed conditions, and show that while efficient convection and mixing require buoyancy, the conditions for rock fracturing, dyke propagation, and occurrence of a new eruption are unlikely to be met if pressure forces are not involved. We suggest that shallow magma chambers at closed conduit volcanoes evolve under essentially pure buoyant conditions over a substantial part of their lifetime, while the generation of a new eruption is associated with sufficient pressure build-up somewhere in the magmatic system.

2 Methods

Pure-buoyant magma chamber replenishment has been previously investigated in detail in Papale et al. (2017). Here we use a similar setup inspired by the Campi Flegrei volcano, a caldera in Southern Italy which hosts part of the same city of Naples, and which is a source of volcanic risk for million people and huge infrastructures in the area (Orsi et al., 2022). Although the Campi Flegrei volcano is a reference for the conditions in these simulations, including overall system geometry and magma compositions, the present results hold a general validity as representative of conditions where a shallow reservoir is connected to a deeper, larger one. Figure 1 shows the setup for the simulations (Papale et al., 2017). The system geometry is constructed in order to be the simplest one holding the fundamental aspects relevant to the analysis. The 2D simulation setup reduces computational costs without loosing the fundamental details on the dynamics within the magmatic system (Garg et al., 2019). The set up includes a large, 8 km deep reservoir hosting shoshonitic magma, connected through a vertical dyke to a shallow, 3 km deep, much smaller reservoir hosting more evolved phonolitic magma. Volatile contents (water and carbon dioxide) are varied within reasonable ranges in order to simulate conditions with variable buoyancy. The volatile content of the deep shoshonite is taken as being the same for all simulations, and variable conditions are obtained by varying, from one simulation to the other, the volatile content of the shallow phonolite (Table 1). The dyke is assumed to initially host the deeper shoshonitic magma, therefore, time zero for all simulations refer to an idealized moment when the deep ascending magma encounters the shallow reservoir. For the simulations with an initial overpressure, that overpressure is applied to the shoshonitic magma at time 0, as if the dyke was reaching the shallow chamber and rupturing the last diaphragm separating the dyke from the chamber. The applied initial overpressure is imposed as a constant surplus with respect to the local, stratified pressure distribution reflecting the non-linear interplay between density, dissolved and exsolved volatile contents, and pressure. The Supplementary Material reports the initial distributions and vertical profiles of relevant quantities.

While the overall system in Figure 1 is closed, the results illustrated below can be seen as describing the open system evolution of the shallow chamber. Accounting for the large system in Figure 1 ensures global consistency of the dynamics in terms of evolution of the conditions characterizing the magma that is injected into the chamber. That leads to the rich dynamics illustrated in this work, and to results that describe in a globally consistent way the evolution over a large magmatic system including the large, deeper regions of magma accumulation. Referring to such a large system has a cost in terms of required computational resources: there are in fact 63742 computational elements in the shallow chamber, increasing to 133,580 when considering the whole simulated domain. As we show below, that computational cost is more than rewarded in terms of consistency of the simulation results and richness of insights into the volcano dynamics. In fact, practically nothing of the complex evolutions described below would be revealed if we aimed at describing magma chamber replenishment without accounting for the interconnections with deeper sub-domains, represented here by a large, deep, less chemically evolved, less degassed magmatic reservoir, and the dyke connecting the deep and shallow reservoirs.

Table 1 illustrates the conditions for the numerical simulations. The two critical parameters for this study are the initial overpressure applied to the shoshonitic magma, and the density difference at the initial magma interface. As explained above, in all simulations the deeper shoshonitic magma is assumed to carry a total (dissolved plus exsolved) volatile content corresponding to 2 wt% total water and 1 wt% total carbon dioxide. Partition between the liquid and gas phases depends on space-time local pressure and temperature conditions, and it is computed with the non-ideal multicomponent saturation model SOLWCAD (Papale et al., 2006). For the three cases with no initial buoyancy (simulation names starting with “N” in Table 1), the total volatile contents in the two magma types are equal. Therefore, in these cases the gas volume fraction and density differences at interface reflect the different saturation conditions due to different melt composition, and the overpressure applied to the shoshonitic magma. In the cases with buoyancy (simulation names starting with “P”) the upper phonolitic magma is assumed to host a lower total volatile content with respect to the shoshonitic magma (Table 1), as it may result from shallow system degassing. The assumed total volatile content in the phonolite, the different overpressure applied in the shoshonite, and the corresponding density modeling and saturation conditions, determine the density of the two magma types at the interface, therefore the magnitude of the initial buoyancy force acting at the interface.

The simulations are made with the in-house finite element code GALES (Longo, Barsanti, et al., 2012; Longo, Papale, et al., 2012; Garg et al., 2018a), which was also employed for the investigation in Papale et al. (2017). The composition employed for the shoshonitic and phonolitic magmas is reported in Table 2. As explained above, multi-component volatile saturation is computed as a function of space and time and depends on local composition, pressure and temperature; density and viscosity are calculated accordingly. (Longo, Barsanti, et al., 2012; C. Montagna et al., 2015; Papale et al., 2017; C. P. Montagna et al., 2022). To keep the computational efforts to within manageable size, the temperature is taken constant (1300 K) throughout the computational domain, and crystallization is neglected (see Discussion).

The code has been recently further developed to improve numerical stability (Garg et al., 2018a), include free surface dynamics (Garg et al., 2018b), fluid-structure interaction dynamics (Garg et al., 2021), and fully 3D dynamics (Garg & Papale, 2022). The reader interested in further details of the mathematics, the numerical methods, and the code stability and performance, is addressed to such papers.

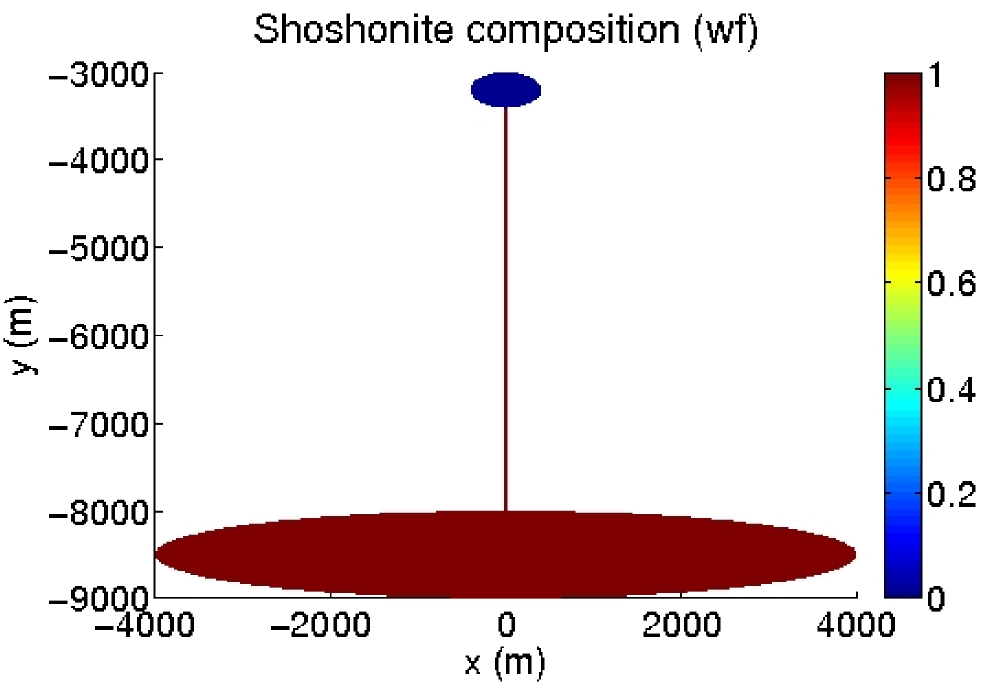

Figure 1. System setup. The system is simplified as being 2D (Cartesian). A shallow elliptical 800 x 400 m reservoir hosting phonolitic magma is connected through a vertical dyke with constant width of 20 m to a deeper and larger (8 × 1 km) reservoir hosting shoshonitic magma. A flat magma interface is placed at shallow chamber entrance. Buoyancy at magma interface is varied by assuming different volatile contents (water and carbon dioxide) in the two magma types. When applied, an initial homogeneous surplus in pressure is imposed to the shoshonitic magma, beyond the initial magmastatic stratification in pressure. The conditions for the executed numerical simulations are reported in Table 1.

Table 1. Simulations performed.

Simulation name	H_2O^T (wt%)$^{(a)}$	CO_2^T (wt%)$^{(a)}$	$\Delta\rho$ (kg/m^3)$^{(b)}$	ΔP (MPa)	Ar$^{(c)}$	Be$^{(d)}$	Be/Ar	Simulation time (s)
P0	1	0.1	162.45	0	$0.60{\cdot}10^9$	0	0	4870
P5	1	0.1	144.50	5	$0.69{\cdot}10^9$	$0.31{\cdot}10^{10}$	4.42	7030
P3.5	1	0.5	92.27	3.5	$0.39{\cdot}10^9$	$0.19{\cdot}10^{10}$	4.85	5340
P6.5	0.77	1	32.05	6.5	$0.06{\cdot}10^9$	$0.16{\cdot}10^{10}$	25.88	5770
N5	2	1	-60.99	5	0	$1.12{\cdot}10^{10}$	-	1570
N10	2	1	-78.39	10	0	$2.25{\cdot}10^{10}$	-	1630
N15	2	1	-93.85	15	0	$3.55{\cdot}10^{10}$	-	1670

$^{(a)}$ Volatile contents refer to the phonolitic magma, whereas for the initially deeper shoshonitic magma these values are $H_2O^T = 2$ wt% and $CO_2^T = 1$ wt% for all simulations.
$^{(b)}$ $\Delta\rho$ corresponds to the density difference between the shallow phonolite and the deep shoshonite, computed at the initial interface.
$^{(c)}$ Archimedes number expressing buoyancy over friction force: Ar$= \rho\Delta\rho g L^3/\mu^2$. Ar=0 when $\Delta\rho < 0$. Magma viscosity μ corresponds to the average viscosity value between the shallow phonolite and the deep shoshonite, computed at the initial interface.
$^{(d)}$ Bejan number expressing pressure over friction force: Be$= \rho\Delta P L^2/\mu^2$.

Table 2. Volatile-free melt composition emplyed in the simulations

	SiO_2	TiO_2	Al_2O_3	Fe_2O_3	FeO	MnO	MgO	CaO	Na_2O	K_2O
Phonolite	53.52	0.60	19.84	1.60	3.20	0.14	1.76	6.76	4.66	7.91
Shoshonite	52.40	0.85	17.60	1.88	5.74	0.12	3.60	7.93	3.43	8.24

Quantities in wt%

3 Results

The simulation results show totally different dynamic situations for the cases where buoyancy is effective ("P" simulations in Table 1) or is absent ("N" simulations). In the following we describe the buoyant cases first, then we consider the not buoyant cases. The focus is initially on the dynamics of shallow chamber replenishment and the relative roles of buoyancy and pressure forces in controlling those dynamics. The overall dynamics down to the deep chamber are described later.

To assess the relative importance of buoyancy and pressure forces, two non-dimensional numbers are employed (see Table 1): Ar or the Archimedes number, representing the ratio between buoyancy and viscous forces; and Be or the Bejan number, representing the ratio between pressure and viscous forces. The Be/Ar ratio indicates therefore the relative roles of pressure and buoyancy forces.

Buoyant systems

Case P0 in Table 1 is similar to the pure buoyant end-member case explored in Papale et al. (2017). Here we briefly summarize the main characteristics of the dynamics, which are fully described in the above paper; and employ them as a reference to compare with the other cases involving both buoyancy and pressure. In general we present the four "P" simulations in order of increasing Be/Ar ratio (Table 1), which corresponds to progressively decreasing buoyancy (but not progressively increasing pressure). The Supplementary Material includes videos showing the evolution of the dynamics in terms of several relevant quantities, for all simulations in Table 1.

When convective motion is triggered by pure buoyancy (case P0), the numerical simulation results show quick disruption of the initial gravitationally unstable interface followed by formation and ascent of intermittent plumes of light magma. Such plumes penetrate into the shallow chamber forming complex circulation patterns which enhance mixing between the two magmas (Figure 2; note that at the resolution of the present simulations, of order 1 m, only mechanical mixing, sometimes referred to as "mingling", is resolved). Injection of light magma into the chamber is accompanied by sinking of the initially resident, partially degassed, denser magma into the dyke. Mixing between the two magmas is mostly effective at dyke level, such that immediately after the very first initial plume no further pure shoshonite enters the chamber. On the contrary, the new plumes after only a few minutes contain at most 50% by weight of the deeper shoshonitic component. The dynamics evolve through a series of discrete plumes of variable size releasing buoyant mixed magma into the chamber, further accompanied by sinking of denser magma into the dyke. A dynamic stratification of composition and properties is built inside the chamber, with the overall stratification continuously disrupted to an extent by new buoyant plumes, then rebuilt until the next plume disrupts it again. For the pure buoyant case, the longer simulations in Papale et al. (2017) show waning of the dynamics for times greater than $4-7$ hours depending on the specific simulation conditions. Beyond those times a condition of dynamic equilibrium is achieved, in which slow dynamics are still ongoing but all macroscopic quantities in the shallow chamber (e.g., the overall mass of components) do not significantly evolve anymore.

When an initial overpressure is added to the rising magma (cases P5, P3.5 and P6.5 in Table 1 and Figure 2), the overall dynamics are qualitatively similar to those described above, dominated by discrete plumes accompanying the overall injection-sinking dynamics. There are, however, important quantitative differences, and most importantly, there are substantial differences in relation to the distribution and evolution of overpressure.

After 250 s from simulation start (left column in Figure 2) there is a well visible plume rising in the shallow chamber in all simulation cases. However, at that time the plume reaches a height in the chamber of only about 100 m for the pure buoyant case P0, whereas that height at the same time is $270-290$ m for the three cases with non-zero overpressure. Thus, the existence of an initial overpressure in the injected magma is seen as a clear push during the first few minutes of simulation. For the two intermediate cases with applied overpressure of 3.5 and 5 MPa, the initial batch of rising magma

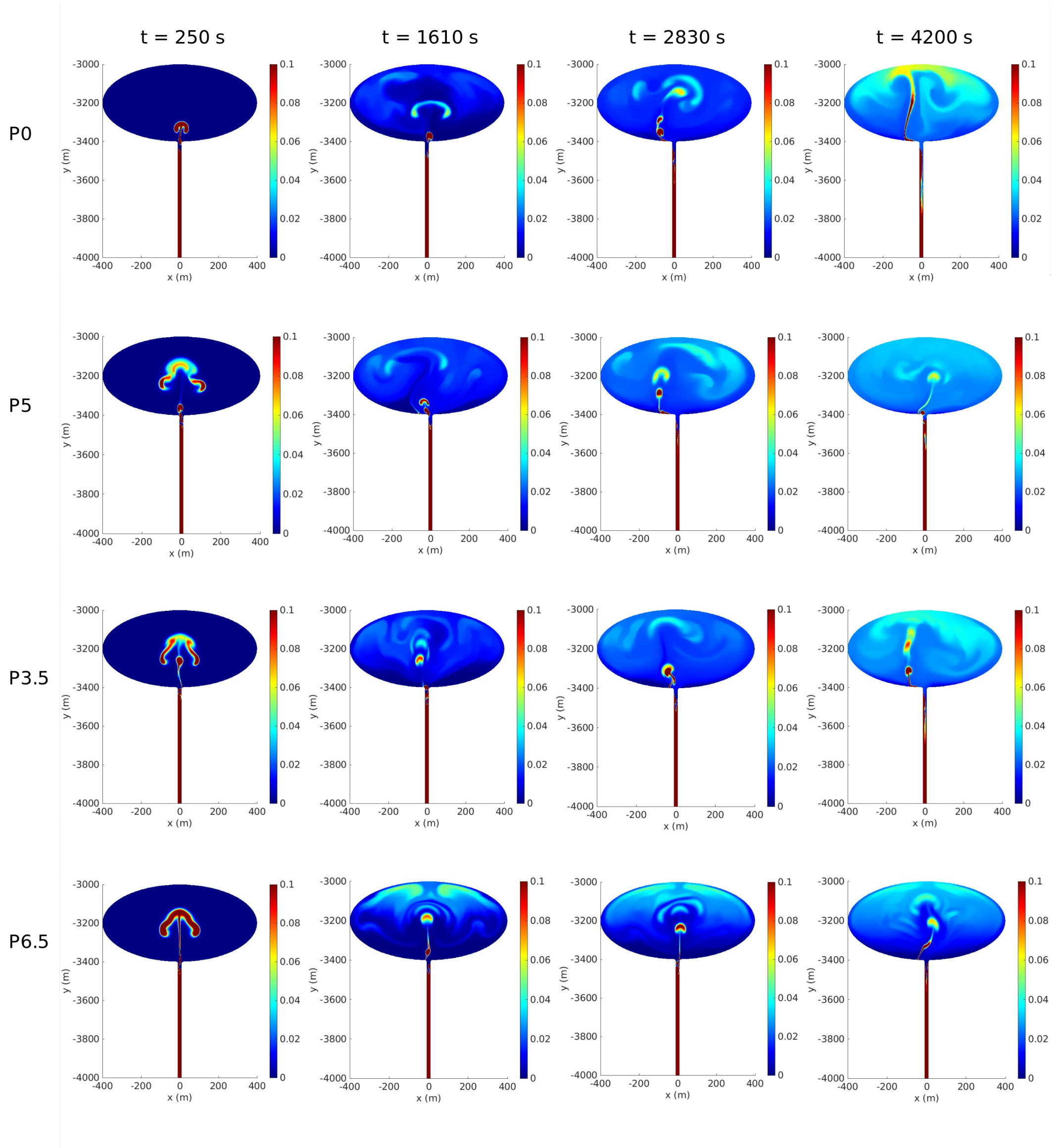

Figure 2. Computed evolution of composition for the buoyant simulation cases. The figures show a zoom view of the shallow chamber and upper portion of the feeding dyke.

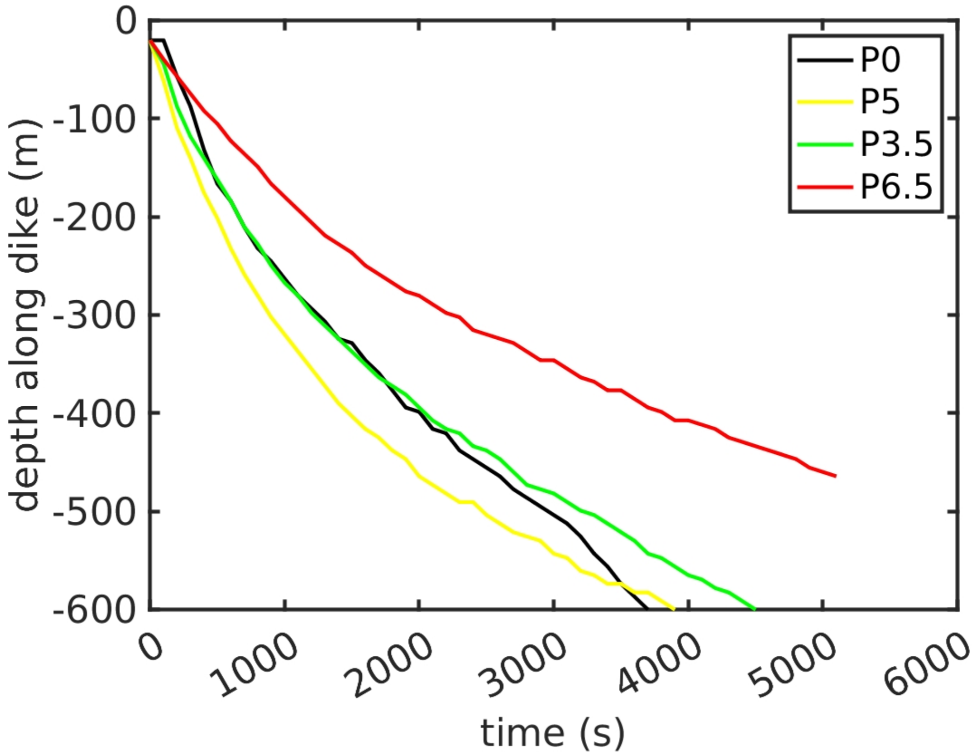

Figure 3. Depth vs time for the front of the magma mixture sinking along the dyke, for the four simulation cases with non-zero buoyancy. Zero on the vertical axis corresponds to chamber entrance level. The initial interface at time zero is at -20 m. The front is taken to correspond to 90% by weight of concentration of the shoshonite.

appears to be formed by at least two individual plumes shortly following one after the other, while for the case with highest overpressure of 6.5 MPa the initial rising batch appears as a well-identified individual plume.

A quantity which looks relevant in illustrating some of the effects and interplays between buoyancy and pressure relates to the motion inside the dyke of the sinking mixture of phonolite and shoshonite. With reference to the pure buoyant case P0, Figure 3 shows that an initial about 150 s are required for the destabilization of the initial gravitationally unstable interface between the two magma types. Once the interface is destabilized, sinking proceeds with the front showing a few velocity oscillations, and a general tendency to reduce velocity with time. After destabilization, the average front velocity in the upper 600 m of dyke is about 16.5 cm/s.

The next two cases examined from Figure 3 are P5 (second most buoyant case, ΔP = 5 MPa, see Table 1) and P3.5 (buoyancy further reduced, ΔP = 3.5 MPa). For both cases i) the initial overpressure produces nearly immediate upward interface displacement (not visible at the scale of the figure, see the Supplementary Material), followed again by sinking of a denser magmatic mixture along the dyke; ii) the sinking velocity is initially larger, then it becomes smaller than for the pure buoyant case; iii) the average sinking velocity in the first 600 m is less than for the pure buoyant case, being 14.4 cm/s for case P5 and 12.7 cm/s for case P3.5. The location where the velocity crossover (from larger to smaller than for the pure buoyant case) occurs varies largely, decreasing in depth with decreasing buoyancy (decreasing Ar in Table 1), from about 585 to 400 m below the shallow chamber when moving from case P5 to P3.5. The trends above are even more evident when moving to case P6.5, for which buoyancy decreases further, while overpressure increases (Table 1). In this case i) the initial upward displacement of the interface is such that the interface penetrates into the chamber during the first 50 s; ii) the crossover with the pure buoyant case occurs at only about 85 m depth; and iii) the average velocity decreases further, so much that the 600 m level below the shallow chamber is never achieved by the sinking magma. Instead, after 5600 s the depth achieved is still less than 500 m. During the time it takes to reach that depth, the average velocity of the sinking magma is of only 8.31 cm/s.

As anticipated above, these trends illustrate the interplay between buoyancy and overpressure in driving the overall dynamics. The increase in overpressure appears to exert an important control on the initial dynamics, as it is exemplified by a stronger push of light magma into the chamber and initially faster rising plume and sinking front. The applied overpressure triggers a more rapid development of the Rayleigh-Taylor gravitational instability (Chandrasekhar, n.d.). However, the long term overall dynamics appear to be more directly controlled by buoyancy, which exerts a strong control on mixing efficiency thus on magma sinking which is its direct reflection. That is evidenced further when analyzing the evolution in time of the overall mass of shoshonite in the shallow chamber (Figure 4). Such a relevant macroscopic quantity results from the complex interplay between injection, mixing, and sinking associated with the different conditions of the simulations. Accordingly, the curves in Figure 4 mimic to an extent those in Figure 3, showing an initial phase where pressure dominates in forcing the shoshonite into the chamber, followed by a longer phase where buoyancy takes the lead and finally dominates in determining the overall efficiency of magma injection. As in the trends in Figure 3, there is a crossover with respect to the pure buoyancy case, which happens sooner for less buoyant conditions. Over the long term, the least effective case in injecting new magma into the shallow chamber is the one (P6.5) associated with the largest overpressure but lowest buoyancy conditions (that is reflected in far less effective mixing for case P6.5 well visible from Figure 2 as a dark blue color over much of the shallow chamber at the longest reported time). That same case was instead the most effective during the initial stages, reflecting the large push by overpressure. The most effective case (P0) is the one with highest buoyancy and lowest (zero) overpressure, which was initially associated to a much less effective injection dynamics (Figures 2 and 4).

The above results are illustrative of the relative roles of buoyancy and overpressure in the efficiency of new magma injection into a shallow chamber. In extreme synthesis, while overpressure dominates initially, the overall process is mostly controlled by buoyancy. However, in terms of likelihood of causing rock fracturing, new dyke injection, and eruption, the existence of an overpressure in the ascending magma is key. That is shown in the following.

Figure 5 shows the evolution of overpressure (defined as the locally computed difference between pressure at current and zero time) in the shallow chamber for the four buoyant simulation cases. Figure 6 illustrates the time evolution of the average shallow chamber overpressure, obtained by weighting the overpressure at any computational node by its corresponding area. The figures highlight macroscopic differences associated with the different conditions in the simulations. The most relevant of such differences is that the sign of the pressure change is negative for the pure buoyant case (P0), and positive for all other cases involving an initially applied overpressure. Counter-intuitive pressure decrease upon chamber replenishment driven by pure buoyancy force is discussed in detail in Papale et al. (2017). In summary, pressure evolution is non-linearly correlated to density and gas volume fraction. While expansion upon gas exsolution exerts a force on the surroundings which contributes to increasing pressure, substitution of dense magma by lighter one implies a net decrease of mass in the chamber and a decrease in the magmastatic pressure contribution, favoring decreasing pressure. For the conditions investigated in Papale et al. (2017) and here, pure buoyancy driven magma injection at shallow level results in either very small (or negligible) increase or significant decrease in overall pressure, with the magnitude of the pressure change increasing with increasing ini-

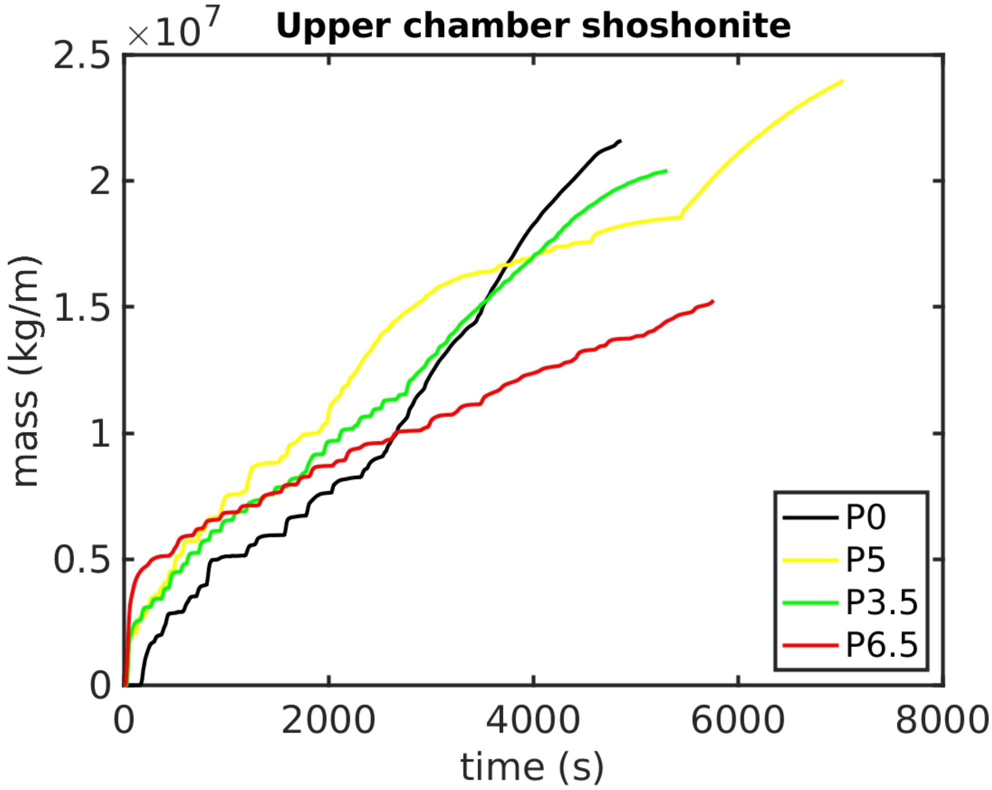

Figure 4. Time evolution of the mass of shoshonite in the shallow chamber, for the four buoyant simulation cases.

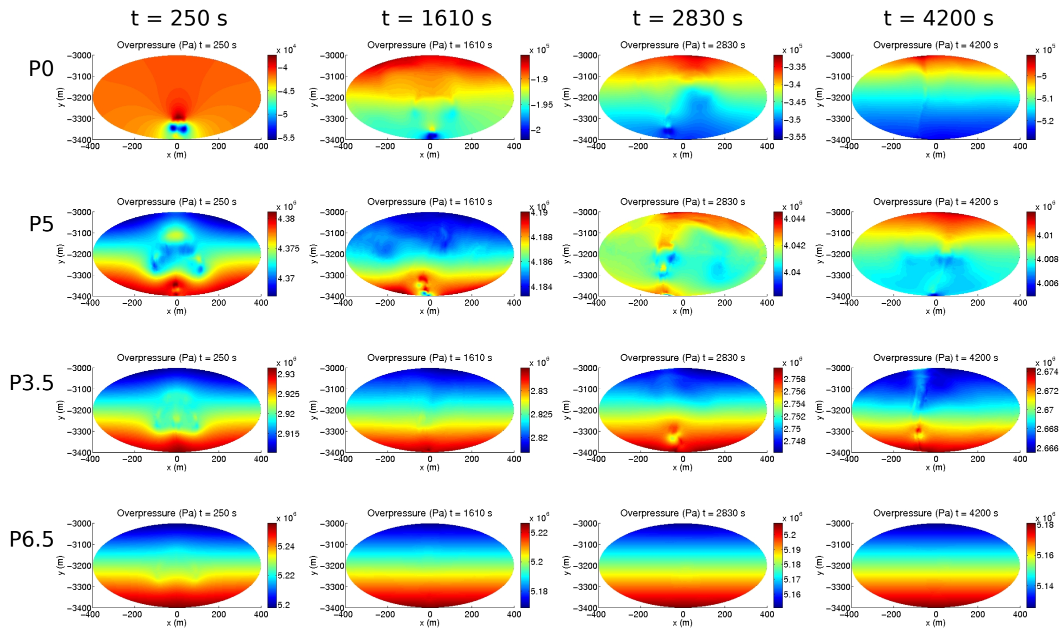

Figure 5. Evolution of overpressure in the shallow magma chamber for the simulation cases with non-zero buoyancy.

tial density difference (thus with increasing Ar in Table 1). Figure 6 shows that for case P0 at the longest simulated time approaching 5,000 s, the average chamber pressure decreases by about 5.5 bars. Because of the magmastatic contribution to pressure decrease, the magnitude of the decrease increases with depth inside the chamber (Figure 5, case P0).

For the three cases with associated overpressure, the pressure change is always positive during the entire simulated times (Figures 5 and 6), although appreciably lower than the applied overpressure. The peak overpressure in the chamber is achieved over a short timescale in the range 10 – 100 s. After that initial pulse the average chamber overpressure slightly and progressively decreases (Figure 6). The extent to which the applied overpressure is transferred into the chamber depends on a number of factors, including magma compressibility which varies from case to case. In the present cases the maximum average overpressure in the chamber is in the range 80-90% of the applied one. Over the times displaced in Figure 6, the maximum overpressure decrease after the initial pressure pulse amounts to 4 – 14% (about 2 to 4 bars) of the achieved peak value.

The above trends depict an initial phase, with time length of order 1 minute, dominated by overpressure, followed by a much longer phase of order hours where buoyancy governs the dynamics causing progressive although limited decrease in overpressure. The applied overpressure is only marginally (10 – 20% for the range of conditions examined here) absorbed by magma compressibility and/or dissipated by internal friction, and largely transferred into the chamber. The longer buoyancy-dominated phase, in all four simulation cases with buoyancy, accounts for chamber pressure decrease by only a few bars, progressively decreasing in magnitude (for the longest simulated times) from 5.5 bars for case P0 with no applied overpressure, to 2.1 bars for case P6.5 with the largest applied overpressure of 6.5 MPa. With reference to the two cases P3.5 and P6.5 where an initial overpressure is associated with least buoyant conditions, during the entire simulation time the overpressure in the chamber decreases from bottom to top (Figure 5). That situation is opposite to that of the pure buoyant case P0, where the overpressure increases

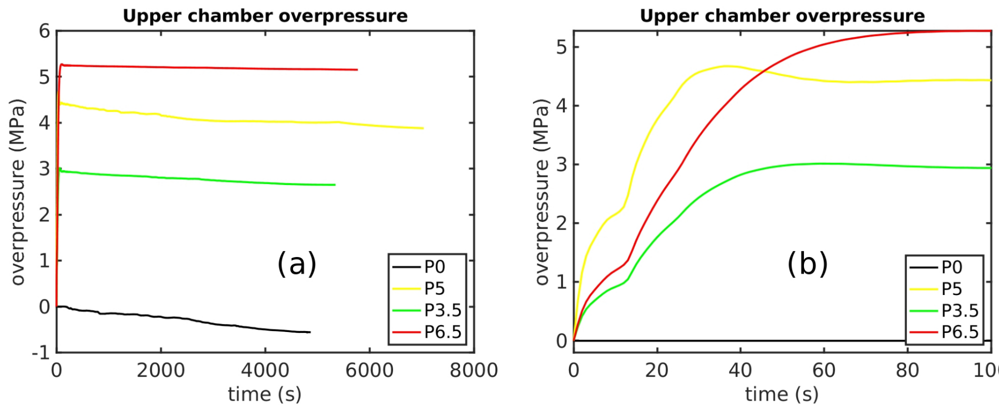

Figure 6. Evolution of the average overpressure in the shallow chamber, for the simulation cases with non-zero buoyancy (cases "P" in Table 1). (a) Evolution over all simulated times. (b) Zoom over the first 100 s.

(it becomes less negative) from bottom to top. The evolution of case P5, which involves both significant overpressure and buoyancy, is peculiar. For this case the evolution during the first about 2000 s is similar to that of the two other cases with overpressure. However, shortly after 2000 s a sort of overturning of the overpressure occurs, causing the distribution of overpressure to become, from there on, similar to that of the pure buoyancy case P0 (overpressure increasing upwards). Once again, the interplay of buoyancy and pressure forces in controlling the dynamics emerges, with the latter causing a downward increase in overpressure, and the former an upward increase (or in other words, both causing a downward increase in the magnitude of the overpressure, with positive sign for pressure force, and negative sign for buoyancy force). Pressure controls the processes initially, then buoyancy becomes dominant. If pressure forces are large enough with respect to buoyancy forces, the downward-increasing pressure-controlled stratification of overpressure is sufficiently stable and it does not get disrupted by subsequent buoyancy control of the dynamics. If instead the relevance of buoyancy increases with respect to the pressure force, then the initially pressure-controlled stratification in overpressure can lead the way to subsequent control by buoyancy, as in the present case P5. Comparison between the cases P5 and P3.5 suggests that such an overturning in the stratification of overpressure may appear for Be/Ar less than about 3.5 (Table 1).

Non-buoyant systems

The simulation cases N5, N10 and N15 in Table 1 do not involve any gravitational instability, as the initial distribution is such that magma density increases everywhere along the direction of gravity. In these cases the dynamics are entirely due to pressure forces, which are applied in the form of an initial overpressure in the initially deeper shoshonitic magma, by 5, 10 and 15 MPa for the three cases above, respectively. Figure 7 (analogous to Figure 2) illustrates the numerical results in terms of distribution of composition. When buoyancy is not acting on the system, the dynamics are very limited. In all three simulated cases there is an initial phase (order a few tens of s) of expansion of the compressed shoshonite into the phonolite, which is in turn compressed, followed by lateral flow of the dense shoshonite over the chamber bottom. The entire dynamics are practically over after a few hundred seconds. After 1000 s no further changes are visible. Mixing is limited to a thin region at the interface between the two magma types. Essentially, the dynamics consist in limited magma intrusion at chamber bottom, accompanied by compression taking 70 – 100 s to achieve a new stable pressure profile in the chamber (Figure 8). As for the buoyant cases seen above, part of the initial overpressure is ac-

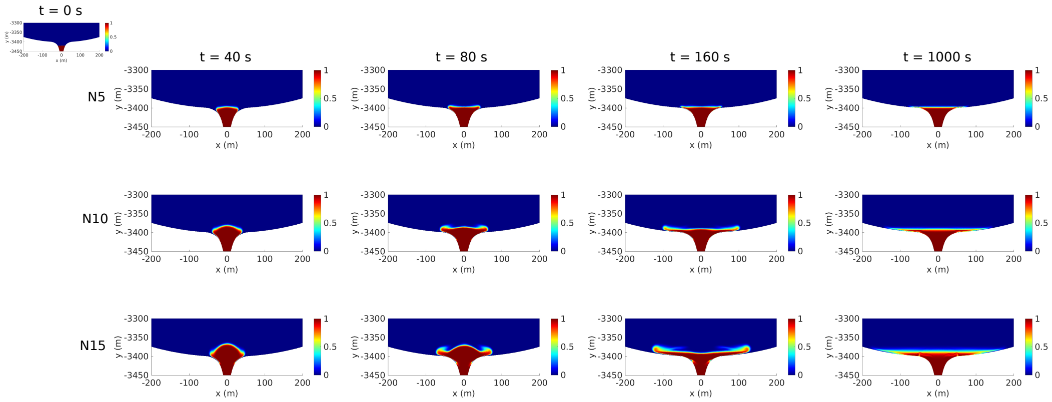

Figure 7. Computed dynamics for the three simulation cases in Table 1 with zero buoyancy. The pictures display zoom views at shallow chamber base, with the colors corresponding to composition. The t = 0 picture for case N5 is equal, in terms of distribution of composition, to the time zero situation for all other cases (in this figure as well as in Figure 2).

commodated by magma compressibility. The proportion of the initially applied overpressure translating into stable chamber overpressure is close to 80% in all three cases (the volatile contents, thus the overall magma compressibility, are also the same for these three simulation cases, see Table 1).

The total mass of shoshonite which is displaced into the chamber (more precisely, displaced above the initial interface) is significantly lower than for the cases with buoyancy, amounting to 3.2, 6.2, and 9 Mkg/m for the three N5, N10 and N15 simulation cases, respectively. By comparison, the P5 case with same initial overpressure as for the N5 case (5 MPa) but buoyancy also associated, injects more than 20 Mkg/m (compared to 3.2) in the first less than 5000 s, and it is still injecting efficiently at that time when the simulation is terminated (Figure 4).

Overall system dynamics

Most of the dynamics for the simulated cases concentrate in the shallow chamber + dyke system, as they are described above. Fluid motion at lower chamber level is very limited or close to null, and the observed evolution at such deep levels is nearly entirely related to pressure, the variations of which are in general important across the entire simulated domain. Pressure propagates across the entire fluid system at the local speed of sound, which depends on isentropic compressibility and is largely controlled by the local volume of gas (in turn controlled by pressure and regulated by real equation of state, contributing to system non-linearity). For the present simulations the speed of sound varies in the range $600 - 1400$ m/s, depending on the specific conditions and generally increasing downwards. Accordingly, a pressure transient originating anywhere in the simulated domain propagates through the entire system in less than 10 s. As a consequence, although the dynamics are negligible in the deep magmatic system, pressure changes at such deep level can be important, causing variations in other important quantities such as dissolved and exsolved amounts of volatiles, gas volume and composition, and magma density and viscosity, reflecting the shallow dynamics dominated by magma intrusion and efficient convection and mixing.

Figures 9 and 10 show the evolution in the entire simulated domain of the horizontally-averaged overpressure, for the simulation cases with buoyancy (Figure 9) and without buoyancy (Figure 10). The overpressure in these figures represents the change with respect to the initial conditions, which included an initially applied overpressure (in all cases

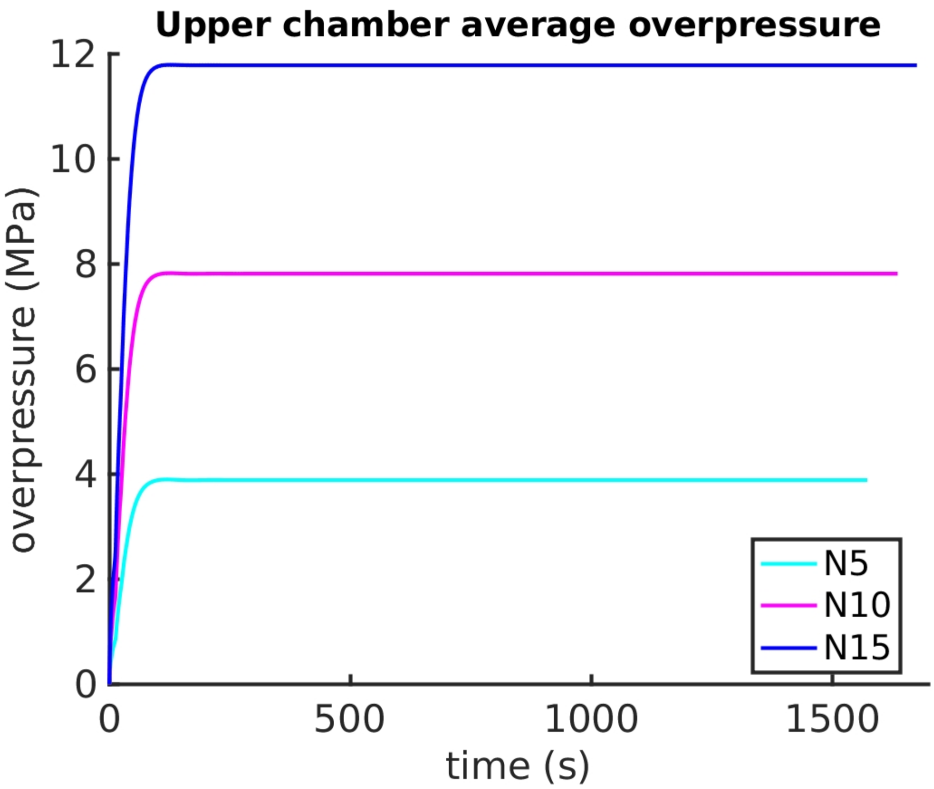

Figure 8. Evolution of the average overpressure in the shallow chamber, for the simulation cases with zero buoyancy and three different applied overpressures (cases "N" in Table 1).

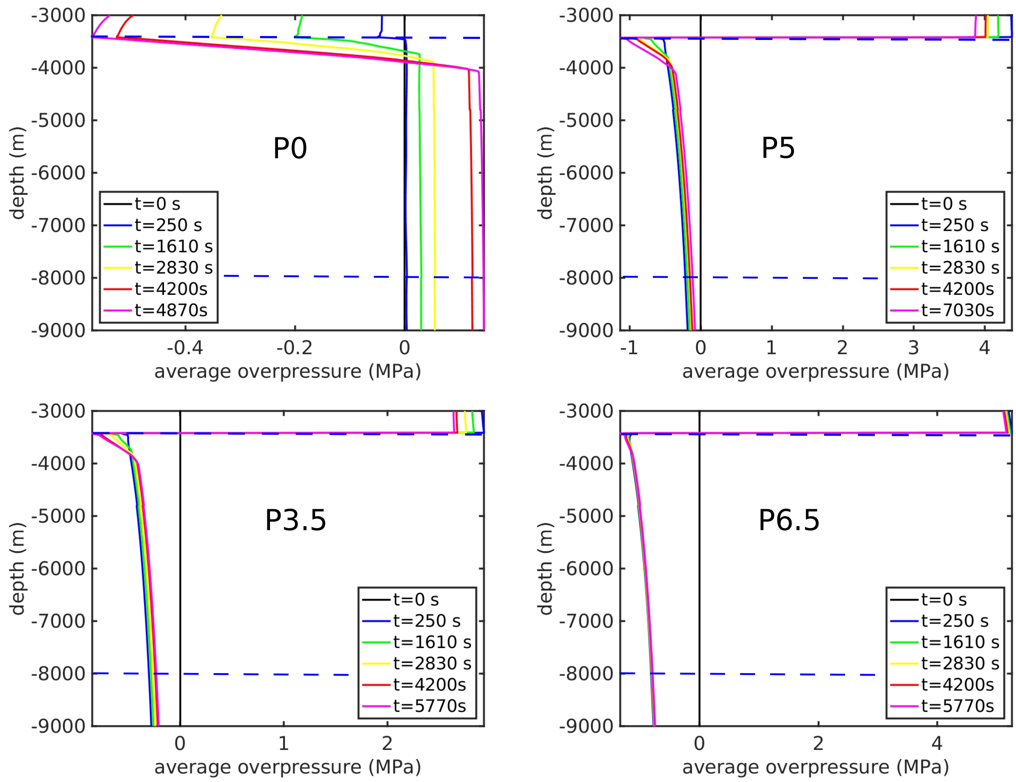

Figure 9. Pressure evolution along the entire system domain, for the four simulations with buoyancy. The lines for each time indicated in the figure represent the horizontally-averaged overpressure. The thick, dashed horizontal blue lines show the extension of the three simulation sub-domains represented by (from the top) the shallow chamber, the dyke, and the deep chamber (see also Figure 1). Note that the overpressure reported here refers to the conditions at time zero, therefore, the initially applied overpressure does not show up.

but case P0 where such an initial overpressure is absent). The most evident feature of the pressure trends in the figures, is that any variation in the upper chamber has a counterpart with opposite sign in the dyke + deep chamber domains. Accordingly, the overpressure in such deep regions is positive for the pure buoyant case P0 for which the overpressure in the shallow chamber is negative, and it is negative for all other cases. For the cases with no buoyancy (Figure 10) the overpressure is more negative for larger initial overpressure (therefore, for larger pressure increase in the chamber). For the cases with buoyancy (Figure 9) that simple relationship does not hold. Instead, the extent of negative overpressure is higher for simulation cases corresponding to larger Be/Ar (larger ratio of pressure to buoyancy force, see Table 1). The trends above suggest that buoyancy by itself, while causing a pressure decrease in the upper chamber, leads to increased pressure in the deeper dyke + chamber system, likely due to compression by the dense, degassed magma sinking along the dyke. Conversely, injection into the shallow chamber of initially pressurized magma, while compressing the chamber, is accompanied by release of the initial overpressure. Whenever buoyancy is a force acting on magma, sinking of dense magma accompanying convection pressurizes the deeper magmatic region, so that the overall pressure evolution at such deep levels depends on the relative importance of pressure and buoyancy forces. In all cases simulated here, with or without buoyancy or pressure forces, the distributions are such that the largest negative overpressure invariably occurs at the junction between dyke and shallow chamber. Increasing the rel-

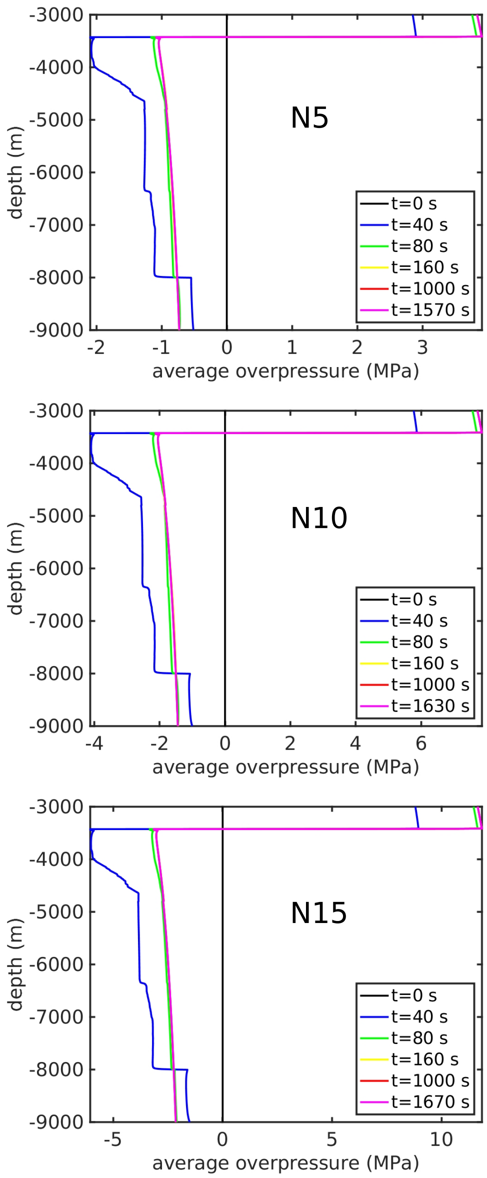

Figure 10. Pressure evolution along the entire system domain, for the three simulations without buoyancy. The lines for each time indicated in the figure represent the horizontally-averaged overpressure. The thick, dashed horizontal blue lines show the extension of the three simulation sub-domains represented by (from the top) the shallow chamber, the dyke, and the deep chamber (see also Figure 1). Note that the overpressure reported here refers to the conditions at time zero, therefore, the initially applied overpressure does not show up.

evance of buoyancy vs. pressure leads to a region at upper dyke level characterized by large gradient of the overpressure (up to > 1 bar every 100 m), which is instead absent in those cases where pressure largely dominates (with the exception of a highly transient initial phase for the zero buoyancy cases, Figure 10, where the pressure gradients largely oscillate).

As it is expected, the size of the different regions plays a role in determining the magnitude of the overpressure. While compression in the shallow chamber amounts to $80 - 90\%$ of the initially applied overpressure, the parallel decompression in the deep chamber is only in the range $5 - 15\%$ of the initial overpressure. In other words, a little relative change in the density, thus in the mass, within the deep chamber, which has a 25x volume per meter with respect to the upper chamber, can accommodate for large density and mass changes occurring at shallow level.

4 Discussion

The present numerical simulations explore the dynamics of shallow magma chamber replenishment under the action of buoyancy and pressure forces. A domain much larger than the shallow chamber is included in the simulations. While each individual sub-domain (shallow chamber, deep chamber, and connecting dyke) is an open system, the entire simulated domain is closed. Such a set up ensures consistency between the shallow evolution and the global dynamics inside a large plumbing system.

The simulation domain is necessarily a simplification of real ones, which are in fact unknown. Further complexities not included in the present analysis may involve the presence of crystals and mushy regions, particularly in the deep magmatic system; the existence of multiple intermediate storage regions connected through complex dyke systems hardly resembling an individual, km-long, vertical one as in the present idealization; the elastic response of the confining rocks to pressure variations in the fluid system; the 3D nature of the real world; and others. Some of the possible roles of such further complexities, including three-dimensionality, domain size and shape, boundary and initial conditions for the simulations, have been discussed in Papale et al. (2017); Garg et al. (2019); Garg and Papale (2022). While there are necessary simplifications, the present results reflect a high level of sophistication in solving the complex physics of magmatic systems, capturing a number of relevant first order aspects of the real world such as the composite nature of magmatic plumbing systems; their compositional heterogeneities with more chemically evolved, partially degassed shallow intrusions; the multi-component nature of the magmatic gas; the complex relationships and feedbacks between magma compositions, volatile contents, magmatic properties, and flow variables and dynamics; the interdependence between processes and dynamics occurring in magmatic sub-domains extending over several km in depth and width; and of specific relevance for the analysis in this work, the diverse roles of buoyancy and pressure forces in driving the dynamics and determining system evolution. In particular, buoyancy and pressure forces are found to originate very different dynamics and exert largely different controls on magma injection dynamics, leading to diverging evolutions. A striking result is that while progressively adding overpressure to buoyant magma translates into similarly progressive changes in overall evolution and dynamics, the transition to non-buoyant, pressurized magma is associated with an abrupt change in the overall dynamics. Although more simulation cases would provide a better representation of the effective range of dynamics, the present results suggest that even little buoyancy is enough to enter a regime where convection and mixing are dominant and effective; while zero buoyancy translates into intrusion at chamber bottom only, with limited or no lateral flow, and limited or no mixing between the injected and resident magmas.

Thus, efficient injection, convection and mixing dynamics strictly require the action of buoyancy. Convection and mixing are invariably accompanied by sinking of dense magma into the feeding dyke. In all simulated cases with buoyancy, efficient magma mixing takes place at upper dyke level, quickly causing the new magma entering the shallow chamber to lose its end-member compositional identity. That happens the faster and more effectively for larger buoyancy with respect to pressure. Pressure and buoyancy forces contribute to the overall system evolution, with the former controlling the short term dynamics, and the latter being more effective over longer times. The evolution of overpressure in the shallow chamber reflects such separate time scales, with an initial fast pressurization amounting to $80 - 90\%$ of the overpressure carried by the deep rising magma, followed by long-term pressure decrease of order a few bars during the subsequent buoyancy-controlled convective phase. Similarly, magma injection shows an initial high rate during the short pressure-dominated phase, followed by a much longer buoyancy-controlled phase with generally lower injection rate depending on the initial density difference thus Ar number in Table 1 (Figure 4).

The above complex evolutions are associated with similarly complex overpressure distributions, that can be highly heterogeneous in the large magmatic domain as well as within individual sub-domains such as the shallow magma chamber. This has important consequences for the associated ground deformation patterns, and requires dedicated analysis to understand potential implications for classical inversion approaches, from simple Mogi models to more complex ones (Mogi, 1958; Gregg et al., 2013; Cannavò, 2019; Zhong et al., 2019).

While buoyancy exerts a dominant control on the occurrence of magma convection and mixing, and in general it controls magma injection at shallow level, there seems to be little chance for a system to evolve towards an eruption without the contribution of pressure forces. Many erupted magmas suggest a rich history of interaction and mixing between different end-members, and the literature abounds with such examples (e.g. Anderson, 1976; Cioni et al., 1995; Griffin et al., 2002; Yang et al., 2007; Zhang et al., 2021; Ji et al., 2021; Alves et al., 2021). Quite often, repetitive magma mixing events are recognized from the analysis of the erupted products, and they are usually interpreted as periodic arrivals of new magma inside a chamber (e.g. Civetta et al., 1991; Cioni et al., 1995; Neumann et al., 1999; Yanagi & Maeda, 1998; Coppola et al., 2017; Caroff et al., 2021). Based on the present results we argue that the common condition likely to dominate much of the history of shallow magmatic bodies is that of periodic arrivals of lighter magma carrying little or no excess pressure, giving rise to efficient convection and mixing and causing limited pressure change, more negative for larger density contrast (larger Ar). Shallow level exsolution of volatiles and magma degassing which largely feeds volcanic plumes and fumaroles, either accompanied or not by cooling and crystallization of magma, provides a universal mechanism for shallow magma density increase. This originates buoyancy forces drawing deeper, less degassed magma towards shallow levels. Under the ubiquitous action of magma degassing at shallow level new batches of volatile-rich, light magma can be periodically brought to shallow levels, partly replacing previously degassed, dense magma sinking down and efficiently mixing with the ascending magma. The present results show that no major pressure changes are associated to such dynamics, which can be therefore maintained over long times, mirrored at the surface by slow ground deformation dynamics from inflation to subsidence.

The ubiquitous process of shallow magma degassing could thus be the controlling factor originating stable conditions for periodic refilling of shallow magma chambers by buoyant magma, giving origin to repeated events of magma mixing similar to those that are observed or reconstructed at virtually any volcano worldwide. Conversely, the occurrence of an eruption requires an important build-up of pressure over a time sufficiently short to escape any attempt by the volcanic system to re-equilibrate at the new conditions. Buoyancy-controlled magma injection dynamics by themselves are unable to achieve such pressure build-up, which instead necessarily requires some other process different from buoyancy and associated convection and mixing. Here we simulate the case where the magma inside the dyke is over-pressurized, mimicking a situation typical for dyke propagation. The simulations involving an initial overpressure may therefore be seen as starting at a time when the last diaphragm separating a rising dyke from a shallow magmatic reservoir is broken. However, our simulations do not investigate the origin of the overpressure. We can speculate on it, by invoking progressive or sudden (e.g., due to an earthquake) accumulation of tectonic stress, transients in magma production rate at depth, deep events associated with magma expansion under confined conditions, etc. Significant overpressure may also be generated directly at shallow level, e.g., due to events causing changes in the relatives rates of magma exsolution and degassing (such as precipitation-induced sealing of confining rocks). In general, however, it seems that pressure build-up requires the occurrence of processes or events less obvious and universal than just shallow magma degassing originating buoyancy. Accordingly, the present results concur to provide a simple explanation for the observed long sequences of repeated shallow magma injection and mixing events which appear to represent the normal condition at most volcanoes worldwide; while the occurrence of a volcanic eruption disrupting such a dynamically stable setup requires the generation of less common conditions leading to sufficient pressure buildup somewhere in the magmatic domain.

5 Open Research

The `GaLeS` numerical code employed for simulations is accessible at `https://gitlab.com/dgmaths9/gales`

Acknowledgments

References

Alves, A., de Assis Janasi, V., de Souza Pereira, G., Prado, F. A., & Munoz, P. R. (2021). Unravelling the hidden evidences of magma mixing processes via combination of in situ sr isotopes and trace elements analyses on plagioclase crystals. *Lithos*, *404*, 106435.

Anderson, A. (1976). Magma mixing: petrological process and volcanological tool. *Journal of Volcanology and Geothermal Research*, *1*(1), 3–33.

Burchardt, S., Galland, O., & Németh, K. (2016). Studying volcanic plumbing systems: Multidisciplinary approaches to a multifaceted problem. *Updates in Volcanology-From Volcano Modelling to Volcano Geology*, 23–53.

Cannavò, F. (2019). A new user-friendly tool for rapid modelling of ground deformation. *Computers & Geosciences*, *128*, 60–69.

Caroff, M., Barrat, J.-A., & Le Gall, B. (2021). Kersantites and associated intrusives from the type locality (kersanton), variscan belt of western armorica (france). *Gondwana Research*, *98*, 46–62.

Cashman, K. V., Sparks, R. S. J., & Blundy, J. D. (2017). Vertically extensive and unstable magmatic systems: a unified view of igneous processes. *Science*, *355*(6331), eaag3055.

Chandrasekhar, S. (n.d.). *Hydrodynamic and hydromagnetic stability.* Oxford Univ. Press, London.

Cioni, R., Civetta, L., Marianelli, P., Metrich, N., Santacroce, R., & Sbrana, A. (1995). Compositional layering and syn-eruptive mixing of a periodically refilled shallow magma chamber: the ad 79 plinian eruption of vesuvius. *Journal of Petrology*, *36*(3), 739–776.

Civetta, L., Carluccio, E., Innocenti, F., Sbrana, A., & Taddeucci, G. (1991). Magma chamber evolution under the phlegraean fields during the last 10 ka: trace element and isotop data. *European Journal of Mineralogy*, 415–428.

Colucci, S., & Papale, P. (2021). Deep magma transport control on the size and evolution of explosive volcanic eruptions. *Frontiers in Earth Science*, *9*, 681083.

Coppola, D., Di Muro, A., Peltier, A., Villeneuve, N., Ferrazzini, V., Favalli, M., . . . others (2017). Shallow system rejuvenation and magma discharge trends at piton de la fournaise volcano (la réunion island). *Earth and Planetary Science Letters*, *463*, 13–24.

Garg, D., Longo, A., & Papale, P. (2018a). Computation of compressible and incompressible flows with a space–time stabilized finite element method. *Computers & Mathematics with Applications*, *75*(12), 4272–4285.

Garg, D., Longo, A., & Papale, P. (2018b). Modeling free surface flows using stabilized finite element method. *Mathematical Problems in Engineering*, *2018*.

Garg, D., & Papale, P. (2022). High-performance computing of 3d magma dynamics, and comparison with 2d simulation results. *Frontiers in Earth Science*.

Garg, D., Papale, P., Colucci, S., & Longo, A. (2019). Long-lived compositional heterogeneities in magma chambers, and implications for volcanic hazard. *Scientific reports*, *9*(1), 1–13.

Garg, D., Papale, P., & Longo, A. (2021). A partitioned solver for compressible/incompressible fluid flow and light structure. *Computers & Mathematics with Applications*, *100*, 182–195.

Gregg, P., de Silva, S., & Grosfils, E. (2013, December 15). Thermomechanics of shallow magma chamber pressurization: Implications for the assessment of ground deformation data at active volcanoes. *Earth and Planetary Sciences Letters*, *384*, 100–108. doi: 10.1016/j.epsl.2013.09.040

Griffin, W., Wang, X., Jackson, S., Pearson, N., O'Reilly, S. Y., Xu, X., & Zhou, X. (2002). Zircon chemistry and magma mixing, se china: in-situ analysis of hf isotopes, tonglu and pingtan igneous complexes. *Lithos*, *61*(3-4), 237–269.

Ji, Z., Ge, W.-C., He, Y., Bi, J.-H., Dong, Y., Yang, H., & Hao, Y.-J. (2021). Mixing of cognate magmas as a process for producing high-silica granites: Insights from guanmenshan complex in liaodong peninsula, china. *Lithos*, *406*, 106495.

Lange, R., & Carmichael, I. S. (1990). Thermodynamic properties of silicate liquids with emphasis on density, thermal expansion and compressibility. *Reviews in Mineralogy and Geochemistry*, *24*(1), 25–64.

Longo, A., Barsanti, M., Cassioli, A., & Papale, P. (2012). A finite element galerkin/least-squares method for computation of multicomponent compressible–incompressible flows. *Computers & fluids*, *67*, 57–71.

Longo, A., Papale, P., Vassalli, M., Saccorotti, G., Montagna, C. P., Cassioli, A., . . . Boschi, E. (2012). Magma convection and mixing dynamics as a source of ultra-long-period oscillations. *Bulletin of Volcanology*, *74*(4), 873–880.

Marsh, B. D. (2015). Magma chambers. In *The encyclopedia of volcanoes* (pp. 185–201). Elsevier.

Mogi, K. (1958). Relations between the eruptions of various volcanoes and the deformations of the ground surface around them. *Bull. Earthquake Res.*, *36*, 99–134.

Montagna, C., Papale, P., & Longo, A. (2015). Timescales of mingling in shallow magmatic reservoirs. *Geological Society, London, Special Publications*, *422*(1), 131–140.

Montagna, C. P., Papale, P., & Longo, A. (2022). Magma chamber dynamics at the campi flegrei caldera, italy. In *Campi flegrei* (pp. 201–217). Springer.

Neumann, E.-R., Wulff-Pedersen, E., Simonsen, S., Pearson, N., Martí, J., & Mitjavila, J. (1999). Evidence for fractional crystallization of periodically refilled magma chambers in tenerife, canary islands. *Journal of Petrology*, *40*(7), 1089–1123.

Orsi, G., D'Antonio, M., & Civetta, L. (2022). *Campi flegrei: A restless caldera in a densely populated area.* Springer Berlin Heidelberg. Retrieved from `https://books.google.it/books?id=QY6EnQAACAAJ`

Papale, P., Montagna, C. P., & Longo, A. (2017). Pressure evolution in shallow magma chambers upon buoyancy-driven replenishment. *Geochemistry, Geophysics, Geosystems*, *18*(3), 1214–1224.

Papale, P., Moretti, R., & Barbato, D. (2006). The compositional dependence of the saturation surface of h2o+ co2 fluids in silicate melts. *Chemical Geology*, *229*(1-3), 78–95.

Papale, P., Moretti, R., & Paonita, A. (2022). Thermodynamics of multi-component gas–melt equilibrium in magmas: Theory, models, and applications. *Reviews in Mineralogy and Geochemistry*, *87*(1), 431–556.

Sparks, R., Annen, C., Blundy, J., Cashman, K., Rust, A., & Jackson, M. (2019). Formation and dynamics of magma reservoirs. *Philosophical Transactions of the Royal society A*, *377*(2139), 20180019.

Sparks, R. S. J., Blundy, J. D., Cashman, K. V., Jackson, M., Rust, A., & Wilson, C. (2022). Large silicic magma bodies and very large magnitude explosive eruptions. *Bulletin of Volcanology*, *84*(1), 1–6.

Sparks, R. S. J., & Cashman, K. V. (2017). Dynamic magma systems: Implications for forecasting volcanic activity. *Elements*, *13*(1), 35–40.

Tibaldi, A. (2015, June). Structure of volcano plumbing systems: A review of multi-parametric effects. *Journal of Volcanology and Geothermal Research*, *298*, 85–135. doi: https://doi.org/10.1016/j.jvolgeores.2015.03.023

Yanagi, T., & Maeda, S. (1998). Magma evolution observed in the matsuura basalts in northwest kyushu, japan: an example of high-pressure open system fractional crystallization in a refilled magma chamber near the crust–mantle boundary. *Physics of the Earth and Planetary Interiors*, *107*(1-3), 203–219.

Yang, J.-H., Wu, F.-Y., Wilde, S. A., Xie, L.-W., Yang, Y.-H., & Liu, X.-M. (2007). Tracing magma mixing in granite genesis: in situ u–pb dating and hf-isotope analysis of zircons. *Contributions to Mineralogy and Petrology*, *153*(2), 177–190.

Zhang, X., Guo, F., Zhang, B., Zhao, L., & Wang, G. (2021, 10). Mixing of cogenetic magmas in the Cretaceous Zhangzhou calc-alkaline granite from southeast China recorded by in-situ apatite geochemistry. *American Mineralogist*, *106*(10), 1679-1689. Retrieved from `https://doi.org/10.2138/am-2021-7786` doi: 10.2138/am-2021-7786

Zhong, X., Dabrowski, M., & Jamtveit, B. (2019). Analytical solution for the stress field in elastic half-space with a spherical pressurized cavity or inclusion containing eigenstrain. *Geophysical Journal International*, *216*(2), 1100–1115.